DNAzyme-amplified DNA Circuit for Highly Accurate MicroRNA Detection and Intracellular Imaging

Hong Wang, Huimin Wang, Qiong Wu, Meijuan Liang, Xiaoqing Liu, Fuan Wang*.

Key Laboratory of Analytical Chemistry for Biology and Medicine (Ministry of Education), College of Chemistry and Molecular Sciences, Wuhan University, Wuhan, P. R. China

[*] To whom correspondence should be addressed. E-mail: fuanwang@whu.edu.cn.

Table of Contents

Table S1. The DNA sequences used to construct the sensing platform

No.	Sequences (5'-3')
Initiator (I)	GAC ACT TCT CTA TCA TTA TCT TGA G
H₁	TCT CTA TCA TTA TCT TGC TTC ATC TTC ATC TCA AGA TAA TGA TAG AGA AGT GTC
H₂	CTT GCT TCA TCT TCA TCT CTC AGT GTC TCT CTA TCA TTA TCT TGA GAT GAA GAT GAA GCA AGA TAA TG
Trigger (T)	GCT TCA TCT TCA TCT CTC AGT GTC
H₃	GAC ACT GAG AGA TGA AGA TGA AGC CAT ACC GCT TCA TCT TCA TCT CTC TAG GCA CCC ATG TAC AGT C
H₄	GCT TCA TCT TCA TCT CTC GTT TTG GAG AGA TGA AGA TGA AGC GGT ATG
H₅	TCA TTC AGC GAT CCT ACA AAA CGA GAG ATG AAG ATG AAG CAA CCA GGC TTC ATC TTC ATC TCT C
H₆	GCT TCA TCT TCA TCT CTC AGT GTC GAG AGA TGA AGA TGA AGC CTG GTT
H₇	TCA ACA TCA GTC TGA TAA GCT AGA CAC TTC TCT ATC ATT ATC TTG AGT CTA GCT TAT CAG ACT GA
miR-21	UAG CUU AUC AGA CUG AUG UUG A
S	FAM-TGA CTG TTrAG GAA TGA C-BHQ-1
H₄Dz	TCA TTC AGC GAT CCT AGC TTC ATC TTC ATC TCT CGT TTT GGA GAG ATG AAG ATG AAG CGG TAT G
H₆Dz	GCT TCA TCT TCA TCT CTC AGT GTC GAG AGA TGA AGA TGA AGC CTG GTT TAG GCA CCC ATG TAC AGT C
Iₐ	GAC TCT TCT CTA TCA TTA TCT TGA G
I_b	GAC TCT TCT GTA TCA TTA TCT TGA G
I_c	GAC TCT TCT GTA TCA TTT TCT TGA G
miR-21-a	UAG AUU AUC AGA CUG AUG UUG A
miR-21-b	UAG AUU AUC AGA UUG AUG UUG A
miR-21-c	UAG AUU AUC AGA UUG AUG AUG A
Let-7a	UGA GGU AGU AGG UUG UAU AGU U
son DNA	ACU CCC AGA UGU UAG CAA C
β-actin mRNA	GCA AGC CAU GUA CGU UGC UAU CCA GGC UGU GCU AUC CCU GU
DNAzyme	TCA TTC AGC GAT CCT ATA GGC ACC CAT GTA CAG TC

Table S2. Comparison of different systems for microRNA detection

System	Reaction time (h)	Sensitivity (M)	Ref.
Target-triggered catalytic hairpin assembly for microRNAs detection	4	3.7×10^{-12}	1
Graphene oxide-assisted CHA circuit	0.5	4.7×10^{-11}	2
HCR-mediated miRNA detection in living cells	4	6.8×10^{-10}	3
HCR-mediated detachment of DNA probe from gold nanoparticles	3	5×10^{-13}	4
DNAzyme-mediated carbolic regeneration of analyte	12	1×10^{-12}	5
DNAzyme-mediated disintegration of magnetic nanoparticles	1 (50 °C)	1.5×10^{-12}	6
Heterologous DNA circuit-mediated miRNA imaging	5	2×10^{-12}	7
C-HCR-mediated nucleic acid detection and miRNA imaging	2	3×10^{-12}	8
DNAzyme-powered cross-catalytic circuit for miRNA detection	5	1.3×10^{-11}	9
CHA-HCR-DNAzyme for miRNA detection and intracellular imaging	4	5.0×10^{-12}	This work

Table S3. The DNA sequences used for CHA-HCR-DNAzyme (H_1) optimization.

No.	Sequences (5'-3')
H_{1a}	CTA TCA TTA TCT TGC TTC ATC TTC ATC TCA AGA TAA TGA TAG AGA AGT GTC
H_{1b}	CTC TAT CAT TAT CTT GCT TCA TCT TCA TCT CAA GAT AAT GAT AGA GAA GTG TC
H_{1c} (H_1)	TCT CTA TCA TTA TCT TGC TTC ATC TTC ATC TCA AGA TAA TGA TAG AGA AGT GTC

Schematic illustration of the upstream CHA system

CHA is the prerequisite for the whole assay, as schematically shown in **Figure S1**. It consists of two hairpins H_1 and H_2. H_1 concludes the sequence b*-a*-d* (5'-3') which is complementary with sequence d-a-b of initiate (**I**). **I** triggers the opening of H_1 by complementary base pairing to yield the DNA assembly **I-H_1** with an exposed single chain a-b-c*. The as-exposed sequence of **I-H_1** could hybridize with H_2 to regenerate **I**, and to produce **H_1-H_2** complex with a newly toehold c*-d* domain (**T**) for triggering downstream HCR. At the same time, the released **I** participates in the next cycle of CHA reaction. Here, **I** can be translated into plenty of substitutions **H_1-H_2** to realize the sensitive detection without undesired systematic fluctuations at the first amplification stage
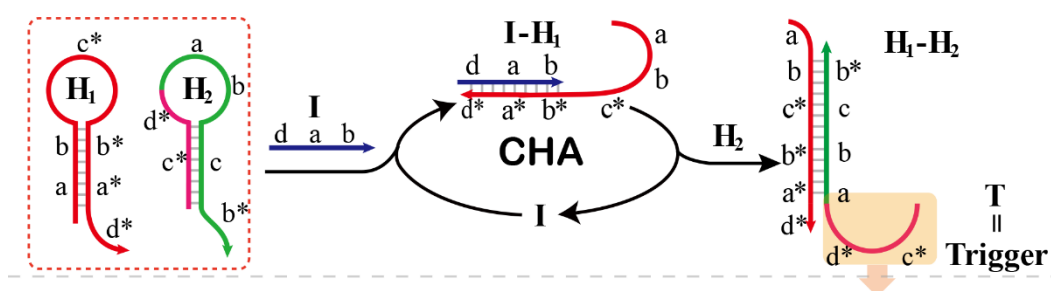

Figure S1. Schematic illustration of the upstream isothermal CHA amplification principle.

Schematic illustration of the downstream HCR system

HCR is composed of four hairpins **H₃**, **H₄**, **H₅,** and **H₆ (Figure S2)**. **H₃** includes the sequence d-c (pink) that can recognize and hybridize with domain c*-d* (**T**) of **H₁-H₂**. **H₄** includes domain c–f* (purple) that is complementary to the sequence f–c* (pink) of hairpin **H₃** while **H₅** includes domain g*–c (pink) that is complementary to the sequence c*–g (purple) of hairpin **H₄**. **H₆** includes sequence c–h* (purple) that is complementary to the sequence h–c* of hairpin **H₅**, and the elongated **T** analog sequence c*–d* (pink). The successively CHA-assembled **T** structure opens **H₃** to assemble an intermediate **T-H₃** structure. The exposed domain f of **T-H₃** docks to **H₄** for yielding intermediate structure **T-H₃·H₄**, of which **H₄** releases hidden single-stranded region c*-g, facilitating its hybridization with **H₅** and producing an intermediate **T-H₃·H₄·H₅** hybrid. The single-stranded sequence g*-c of the opened **H₅** again binds and unfolds **H₆** to construct an intermediate **T-H₃·H₄·H₅·H₆** hybrid, restoring an exposed single-stranded sequence c*-d* in **H₆** with an analog sequence of the structure **T**. Thus, the exposed sequence of **H₆** again opens **H₃** and leads to HCR-involved multiple assembly of **H₃**, **H₄**, **H₅** and **H₆** into a polymeric nanowire consisting of **T-(H₃·H₄·H₅·H₆)n** and realizes the amplification of the indirect target **T** detection in the second step.
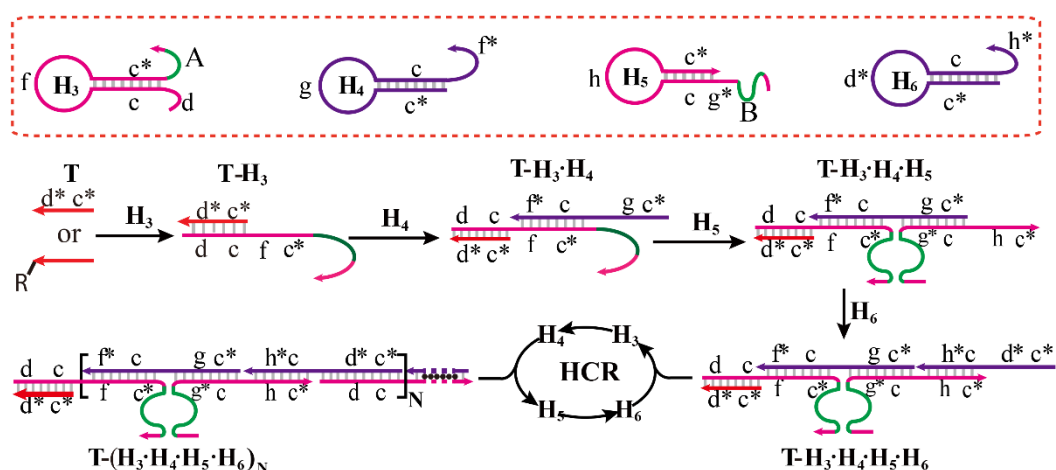

Figure S2. Schematic illustration of the downstream isothermal HCR amplification principle.

AFM characterization of CHA-HCR-DNAzyme mixture

The supramolecular copolymer product of CHA-HCR-DNAzyme amplifier can't generate without initiators. To further demonstrate it, atomic force microscopy (AFM) was carried out to investigate the mixture hairpins of CHA-HCR-DNAzyme system without activating. Only tiny spots are observed without any assembled products for the non-activated CHA-HCR-DNAzyme system (**Figure S3**), suggesting that no undesired hybridization occurred between these hairpin components.
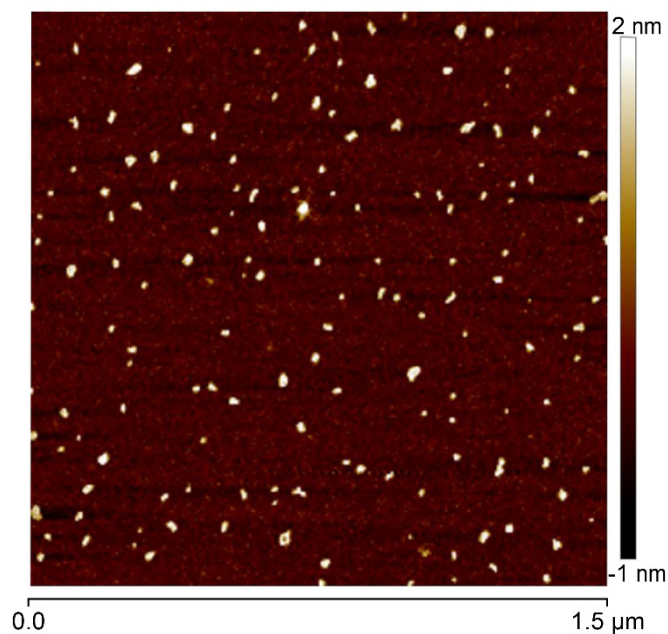

Figure S3. AFM characterization of the non-activated CHA-HCR-DNAzyme reactants.

Demonstration of the retained activity of the HCR-assembled DNAzyme

The supramolecular copolymer product of CHA-HCR-DNAzyme amplifier has been exemplified by 9% PAGE experiment. To further demonstrate the feasibility of the proposed strategy, the fluorescence experiment was carried out to investigate the re-assembled DNAzyme activity of our CHA-HCR-DNAzyme system for effective signal transduction. The fluorescence experiment was thus carried out to investigate the re-assembled DNAzyme of our CHA-HCR-DNAzyme system for effective signal transduction. As seen from **Figure S4**, the H_6-excluded HCR-DNAzyme system could generate in principle 50 nM of reassembled DNAzyme with 50 nM T since it was encoded with a 1:1 amplification efficiency. As expected, the H_6-excluded HCR-DNAzyme (lane b) shows an approximately equal fluorescence response of the 50 nM intact DNAzyme (lane c), demonstrating that the reassembly of split DNAzyme could still retain a high catalytic cleavage activity. In addition, the intact HCR-DNAzyme system revealed a much higher fluorescence readout with 50 nM trigger **T** (lane a), demonstrating the feasibility of our proposed split DNAzyme re-assembly strategy, and the efficient HCR-amplified DNAzyme formation.
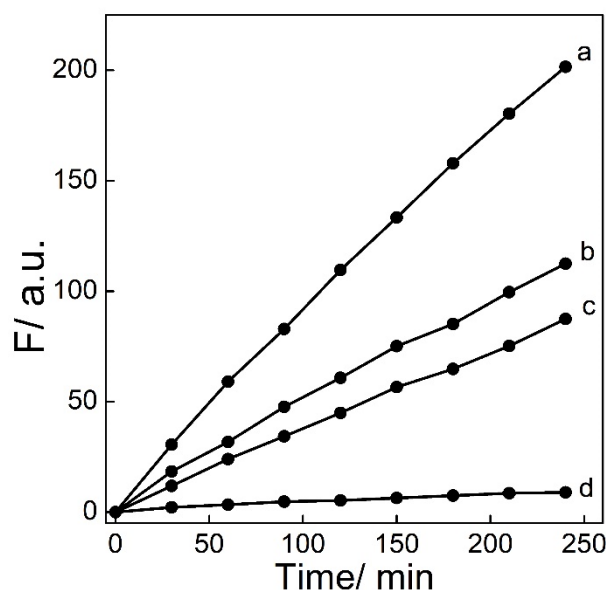

Figure S4. Time-dependent fluorescence changes (λ=520 nm) of the DNAzyme reaction from different DNAzyme-assembly mode: (a) HCR-DNAzyme, (b) H_6-excluded HCR-DNAzyme, (c) intact DNAzyme (50 nM), and (d) no DNAzyme.

Demonstration of the indispensable role of each CHA-HCR-DNAzyme reactant

Hairpin-excluded experiment of CHA-HCR-DNAzyme is outlined in **Figure S5**. When H_1, H_2, and H_4 are excluded from the triple cascading CHA-HCR-DNAzyme system, almost no obvious fluorescence differences are observed whether there is an initiator or not (black curves). And lines b* (blue) is the absence of H_6 experiments with initiator. As seen from the principle scheme, HCR is incomplete without H_6, but CHA-DNAzyme could operate as usual. So here a fluorescence-enhanced dynamic line b* is observed with a slightly higher value compared to its' control experiment without initiator (line b). Line a* is the intact system with all the six hairpins, with a dramatic fluorescence enhancement. This hairpin-excluded experiment demonstrates that the CHA-HCR-DNAzyme circuit conjugated as anticipated and it's metastable enough without signal leakage.
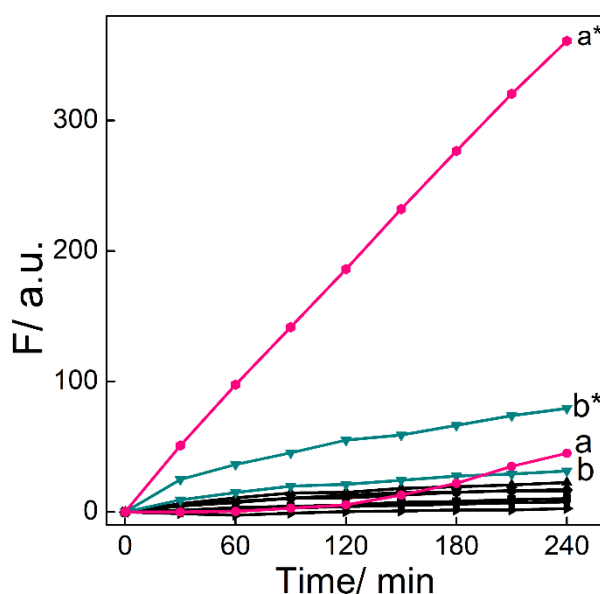

Figure S5. Time-dependent fluorescence changes ($\lambda=520$ nm) of CHA-HCR-DNAzyme system excluding H_1, H_2, H_4, and H_6 from the system. Data a*/a (pink lines) is the whole system with all the hairpins with/without 50 nM initiator. Data b*/b (blue lines) is the system without H_6. No obvious fluorescence difference was observed between them for the other experiments (marked with black).

Optimization of CHA-HCR-DNAzyme reaction *via* H_1

To decrease the system leakage and realize a better signal to background ratio (S/B) mentioned above, the sequence of H_1 is optimized to improve the background fluorescence and reaction rate, which plays a paramount role in the CHA-HCR-DNAzyme system. Here we design three H_1 sequences (H_{1a}, H_{1b}, H_{1c}), whose stem bases are 14, 16, 17 respectively (**Table S3**). **Figure S6**A shows the NUPACK fitting for H_1, and the blue circle is optimized position. The fluorescence signal goes up with the stem base decreasing both in the experimental (a*, b*, c*) and control group (a, b, c) (**Figure S6**B). A serious fluorescence leakage is observed with 14 base pairs in the stem of H_1 (line a). To ensure certain reaction rate (based on S/B), the final sequence of H_1 for the target DNA detection is H_{1c}.
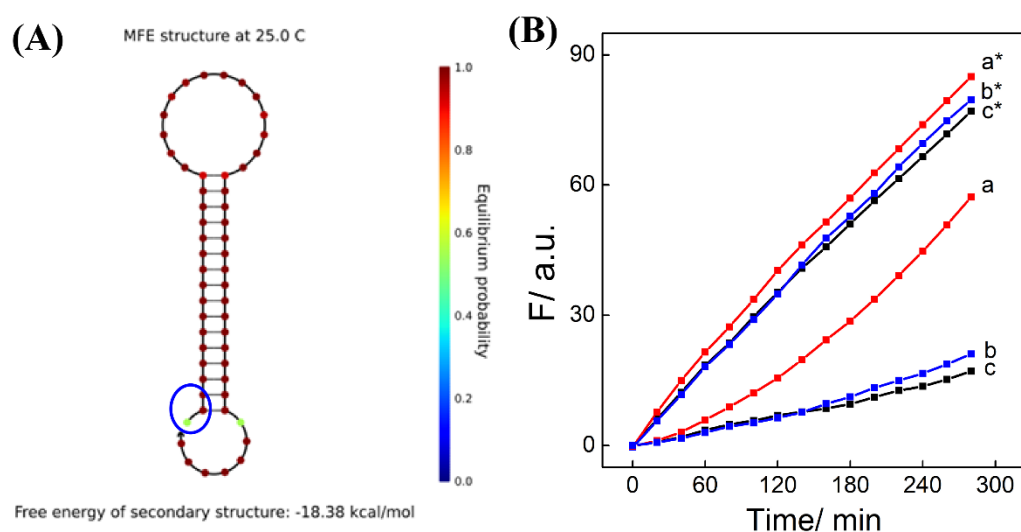

Figure S6. The optimization of H_1: (A) The NUPACK fitting for H_1; (B) Time-dependent fluorescence changes (λ=520 nm) upon analyzing I with different H_1, a*/a for H_{1a}; b*/b for H_{1b}; c*/c for H_{1c}.

Optimization of CHA-HCR-DNAzyme system *via* DNAzyme

The DNAzyme-grafting efficiency was investigated. Similar with HCR hairpins H_3 and H_5, the other two hairpins H_4 and H_6 were also integrated with the split DNAzyme subunits to get H_{4Dz} and H_{6Dz}, respectively. And the revised HCR-DNAzyme was nominated as HCR-bis-DNAzyme. Thus the revised HCR could in principle assemble twice amount of DNAzyme units than the present HCR-DNAzyme system (**Figure S7**A). To our surprise, there is no further signal amplification for the revised CHA-HCR-bis-DNAzyme system. The CHA-HCR-bis-DNAzyme system showed lower signal amplification (lane b*, **Figure S7**B) than the present CHA-HCR-DNAzyme system (lane a*, **Figure S7**B) for analyzing 1 nM of initiator. The steric hindrance of the newly introduced DNAzyme-subunits-grafted hairpin might play a key role for this limited amplification efficiency. That means the cross-hybridization rate and completeness of our HCR could be tremendously slowed down by the DNAzyme grafting fragments which could not be compensated by the doubly assembled DNAzyme. As a result, the single-DNAzyme-subunit-integrated hairpin H_3 and H_5 are chosen as the final design for our triple CHA-HCR-DNAzyme system.
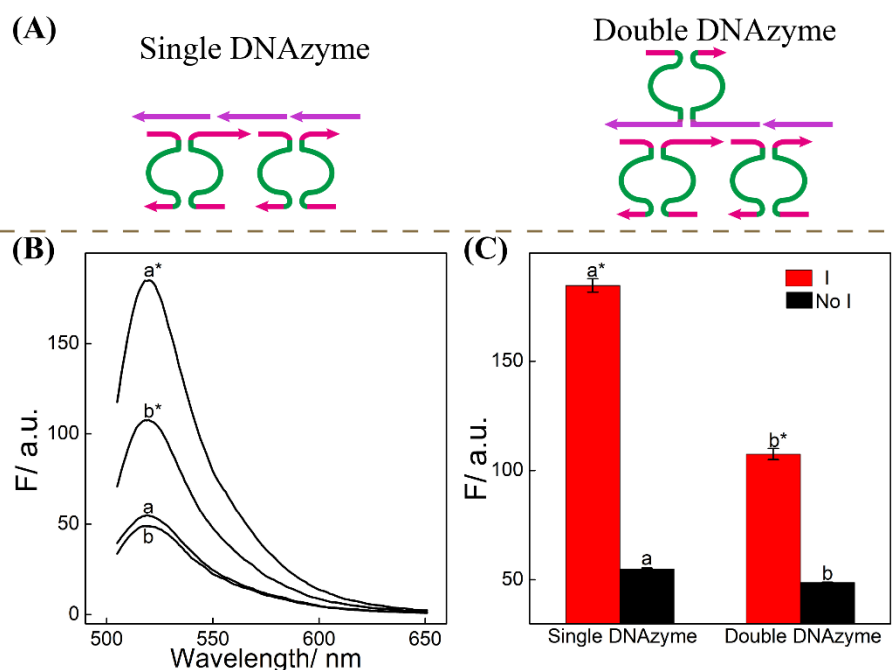

Figure S7. (A) Schematic illustration of the single HCR-DNAzyme and double HCR-bis-DNAzyme systems. (B) Fluorescence behaviors of the CHA-HCR-DNAzyme system with (a*) and without (a) initiator (1 nM), and the CHA-HCR-bis-DNAzyme system with (b*) and without (b) initiator (1 nM) after a fixed time-interval of 4 h. (C) Bar representation of the fluorescence intensity changes ($\lambda = 520$ nm) in (B).

Concentration optimization of CHA-HCR-DNAzyme system

Under the feasible conditions, the hairpin concentrations are optimized (**Figure S8**). The initial incubation of CHA-HCR-DNAzyme mixture is 200 nM for each hairpin with 50 nM initiator I, which shows an obvious fluorescence increase with the signal-to-background ratio of ~14-fold (data c, **Figure S8**). Much more substrates are cleaved with higher hairpin concentration for a stronger signal readout in principle. However, the system leakage will be serious because of the unstable of hairpins inevitably. Increasing all the hairpins to 400 nM leads to dramatically signal decrease (data d, **Figure S8**). Much lower signal-to-background ratio is observed with 400 nM H_1 and H_2 when the concentration of HCR hairpins is 200 nM (data e, **Figure S8**). H_1 is the beginning of the whole circuit, whose down-regulation can reduce the background signal efficiently. Meanwhile, H_2 with an analog sequence of T is the origin of HCR and DNAzyme cleavage. On one hand, the background will be down obviously without enough H_2. While on the other hand, Decreasing the concentration of H_2 would reduce the displacement efficiency of CHA with a signal amplification decline (data a and b, **Figure S8**). From the above, the final optimum hairpin mole ratio of H_1, H_2, and HCR was 1:2:2 namely 100 nM H_1, 200 nM H_2, H_3, H_4, H_5, H_6 with the signal-to-background ratio ~15.6-fold.
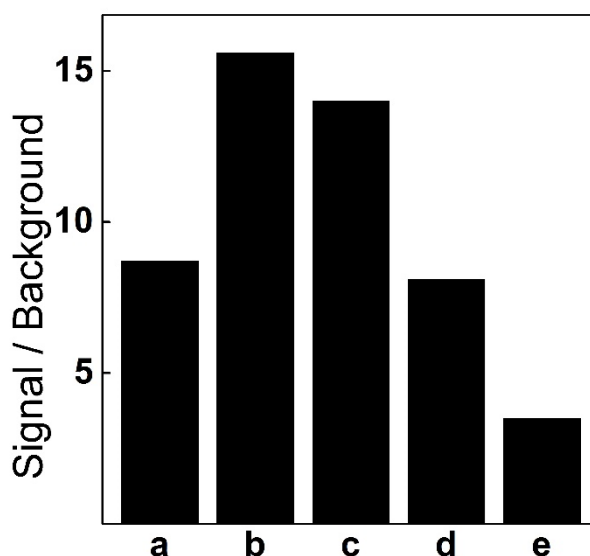

Figure S8. Signal to background ratio of the hairpin concentration optimization of the CHA-HCR-DNAzyme system：(a) 100 nM H_1, 100 nM H_2, 200 nM H_3, H_4, H_5, H_6; (b) 100 nM H_1, 200 nM H_2, 200 nM H_3, H_4, H_5, H_6; (c) 200 nM H_1, 200 nM H_2, 200 nM H_3, H_4, H_5, H_6; (d) 400 nM H_1, 400 nM H_2, 400 nM H_3, H_4, H_5, H_6; (e) 400 nM H_1, 400 nM H_2, 200 nM H_3, H_4, H_5, H_6.

Fluorescence monitoring these different dual amplifiers

Time-dependent fluorescence measurements for H_6-expelled CHA-DNAzyme (**Figure S9**A), and HCR-DNAzyme (**Figure S9**B). Both show liner growth over reaction time for the peak intensities. But their detection limits are only down to 1 nM. CHA-HCR-DNAzyme circuit provides ~3-fold higher amplification efficiency than the CHA-DNAzyme system and ~1.7-fold than HCR-DNAzyme with 50 nM initiator I, indicating the subsequent growth of the HCR polymers along the CHA assemblies. Compared with various concentrations of initiator I, CHA-HCR-DNAzyme system shows great advantages at the lower concentration, further revealing that the triple combination of CHA, HCR and DNAzyme realizes synergistic signal amplification.
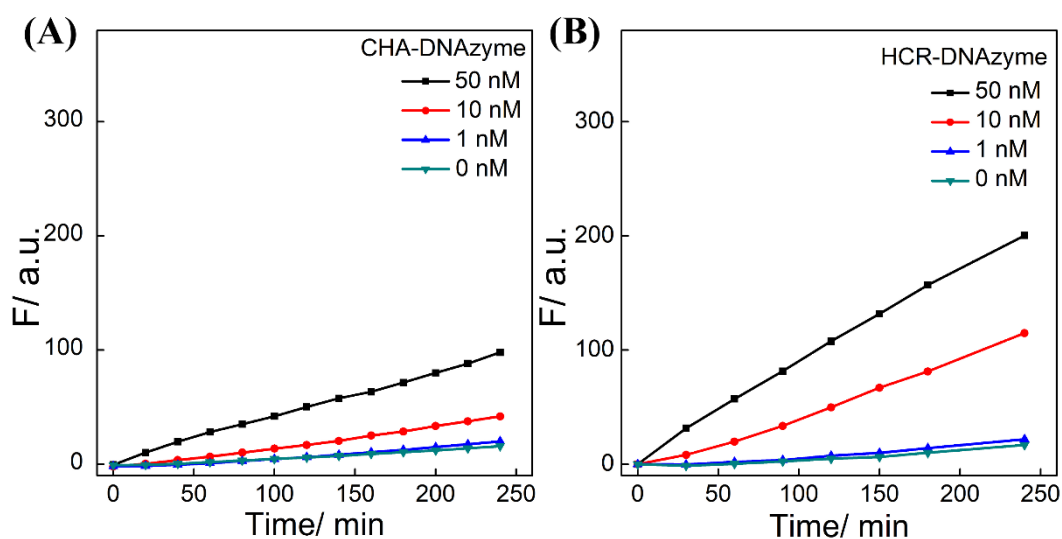

Figure S9. Time-dependent fluorescence changes (λ=520 nm) versus different concentrations of initiator. (A) by the CHA-DNAzyme circuit; (B) by the HCR-DNAzyme circuit.

Selectivity of the CHA-HCR-DNAzyme system

Selectivity of the CHA-HCR-DNAzyme system was examined using one-, two-, and three-base mutant DNA targets I_a, I_b, and I_c (**Figure S10**). The obtained fluorescence intensity exhibited little enhancement to the background for I_a, I_b, and I_c mutant initiators, implying that the CHA-HCR-DNAzyme system affords high selectivity with the ability to discriminating base mutations.
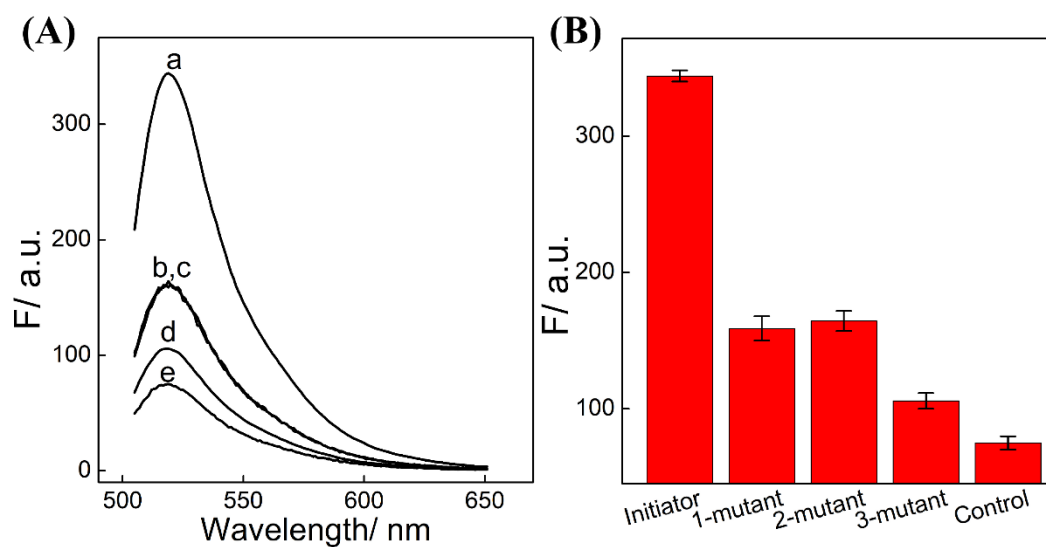

Figure S10. (A) Fluorescence spectrum (λ=520 nm) of the CHA-HCR-DNAzyme sensing system with different analytes for four hours: (a) I, 50 nM, (b) I_a, 50 nM, (c) I_b, 50 nM, (d) I_c, 50 nM, and (e) no analytes. (B) Summary of the fluorescence results.

Selectivity of the miR-21-targeting CHA-HCR-DNAzyme system

The selectivity of the miR-21-analyzing system was also explored by choosing several representative interference nucleic acids, including β-actin mRNA, son DNA and let-7a miRNA. As shown in **Figure S11**, only miR-21 reveals a dramatically increased fluorescence transduction (curve a), and all of these interfering RNAs generate no obvious fluorescence response (curves b, c, and d) that is approximately equal to the blank control without an initiator (curve e). This indicates the high selectivity of our newly established CHA-HCR-DNAzyme-amplified miR-21 detection strategy.
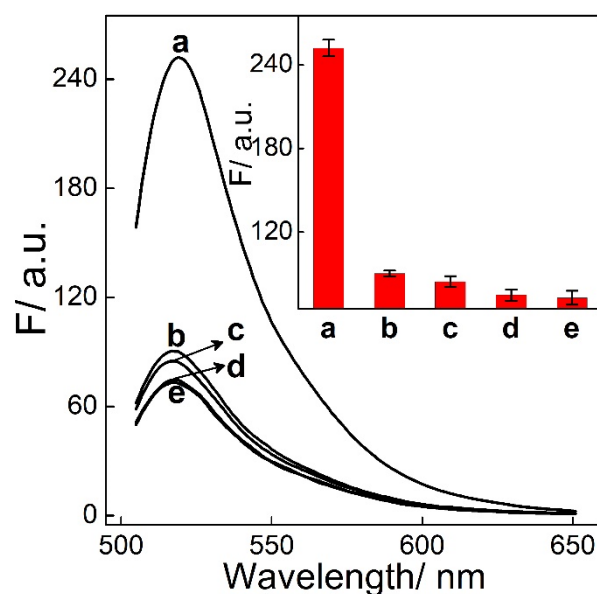

Figure S11. Fluorescence behaviors of the updated CHA-HCR-DNAzyme system in the presence of different analytes: (a) miR-21, (b) β-actin mRNA, (c) son DNA, (d) let-7a, and (e) no analyte. Inset: Bar representation of the fluorescence intensity changes ($\lambda = 520$ nm).

CHA-HCR-DNAzyme-based miR-21 imaging

As shown in **Figure S12**, to further emphasize the miR-21 targeting CHA-HCR-DNAzyme system in different living cells, Hela cells were introduced as a low miR-21 expression control, and MRC-5 cells were introduced as an important negative control since it was encoded with no miR-21 expression. Obvious fluorescence signal is observed in live MCF-7 cells (sample A), indicating a higher miR-21 expression level in MCF-7 cells than HeLa cells (sample B). MRC-5 cells (sample C) show little fluorescence signal. These results show that the CHA-HCR-DNAzyme system can distinguish different cell lines based on their different endogenous miRNA expressions.
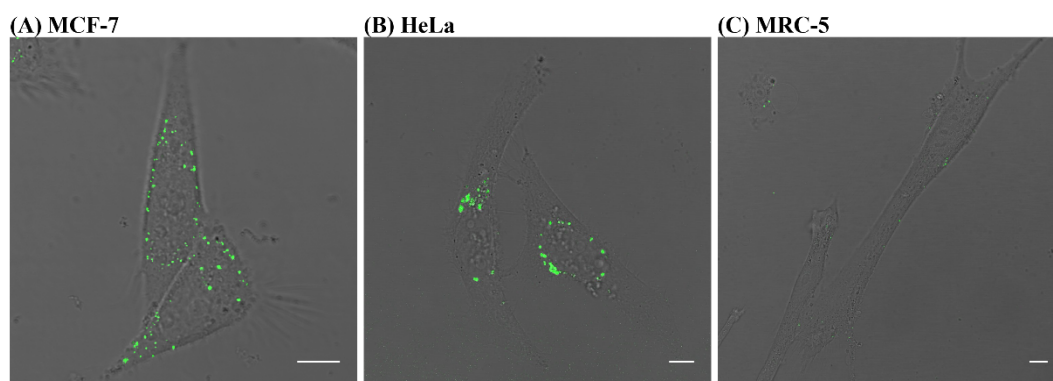

(A) MCF-7 **(B) HeLa** **(C) MRC-5**

Figure S12. Living cell analysis of miR-21 based on CHA-HCR-DNAzyme strategy. Confocal laser scanning microscopy (CLSM) imaging of miR-21 in (A) routine MCF-7 living cells, (B) HeLa, and (C) MRC-5 living cells by the CHA-HCR-DNAzyme amplifier. All of the mentioned living cells were transfected and incubated with miR-21-targeting CHA-HCR-DNAzyme mixture at 37 °C for 4 h. All scale bars correspond to 10 μm.

Control experiments of intracellular miR-21-imaging system

To demonstrate the high amplification efficiency of the CHA-HCR-DNAzyme system for miR-21 imaging, intracellular control experiments were carried out by removing one of the hairpin components from the CHA-HCR-DNAzyme mixture. As shown in **Figure S13**, obvious fluorescence spots were acquired for CHA-HCR-DNAzyme system (sample a), while reduced spots were observed for multiple CHA – DNAzyme imaging system (H_6-excluded CHA-HCR-DNAzyme mixture, sample e). Moreover, almost no fluorescence spots appeared in sample b, c, d, which was H_1 -, H_2 - or H_4 -excluded CHA-HCR-DNAzyme system respectively, indicating that all of the hairpin reactants were indispensable for the present CHA-HCR-DNAzyme circuit, especially in living cells.
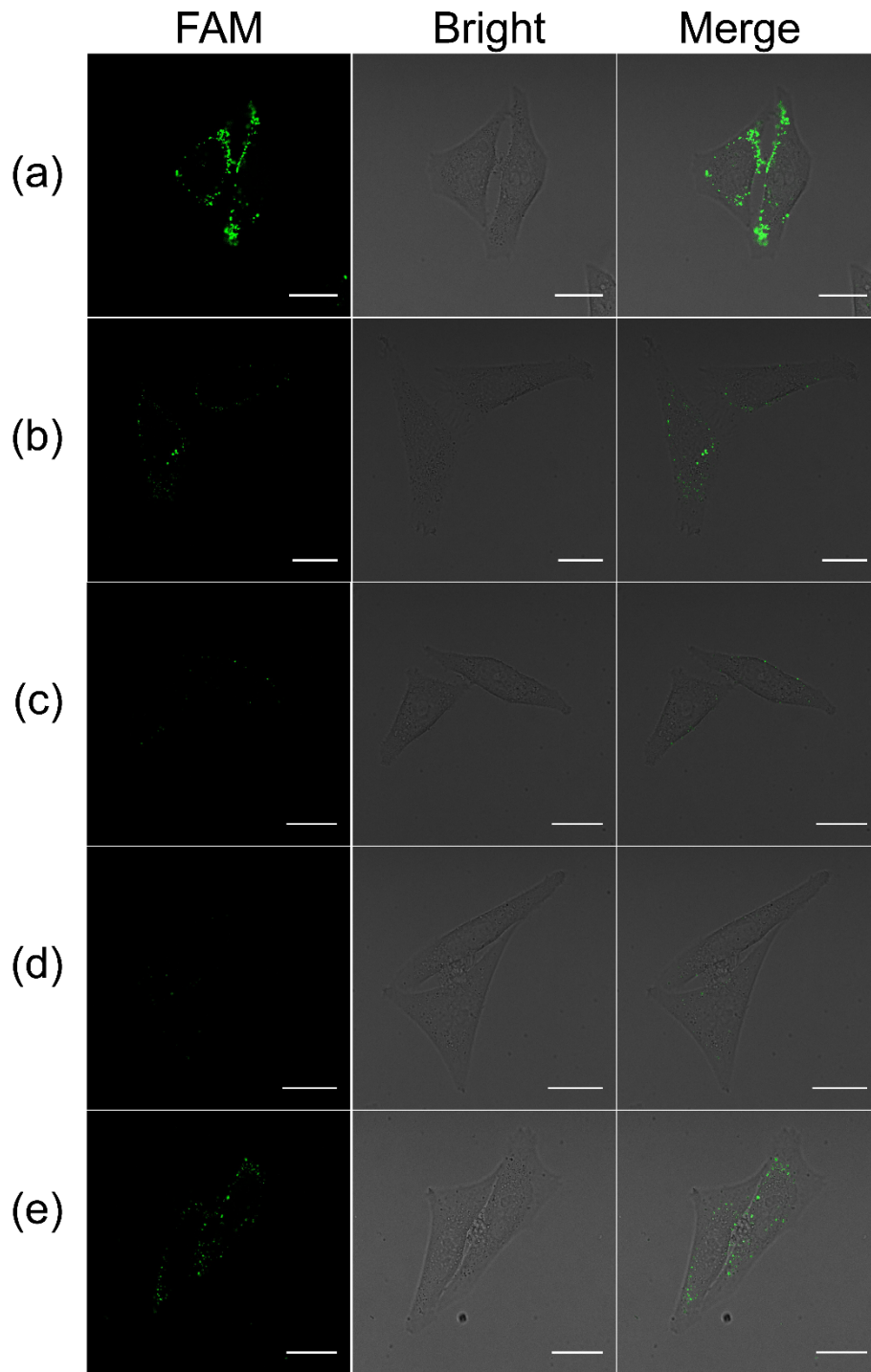
Figure S13. Confocal laser scanning microscopy imaging of miR-21 in MCF-7 living cells which were transfected with (a) the intact CHA-HCR-DNAzyme system, (b) H_1-excluded CHA-HCR-DNAzyme system, (c) H_2-excluded CHA-HCR-DNAzyme system, (d) H_4-excluded CHA-HCR-DNAzyme system and (e) H_6-excluded CHA-HCR-DNAzyme system at 37 °C for four hours. Scale bars correspond to 20 μm.

Reference

(1) D. Li, Y. Wu, C. Gan, R. Yuan, and Y. Xiang, *Nanoscale*, 2018, **10**, 17623-17628

(2) S. Zhen, X. Xiao, C. H. Li and C. Huang, *Anal. Chem.*, 2017, **89**, 17, 8766-8771

(3) F. Yang, Y. Cheng, Y. Cao, H. Dong, H. Lu, K. Zhang, X. Meng, C. Liu and X. Zhang, *Chem. Sci.*, 2019, **10**, 1709-1715

(4) Z. Wu, G. Liu, X. Yang and J. Jiang, *J. Am. Chem. Soc.*, 2015, **137**, 6829-6836.

(5) F. Wang, J. Elbaz, C. Teller, and I. Willner, *Angew. Chem. Int. Ed.,* 2011, **50**, 295-299.

(6) B. Tian, Y. Han, E. Wetterskog, M. Donolato, M. F. Hansen, P. Svedlindh and M. Strömberg, *ACS Sens.*, 2018, **3**, 1884-1891.

(7) H. Wang, C. Li, X. Liu, X. Zhou, and F. Wang, *Chem. Sci.* 2018, **9**, 5842-5849.

(8) J. Wei, X. Gong, Q. Wang, M. Pan, X. Liu, J. Liu, F. Xia and F. Wang, *Chem. Sci.*, 2018, **9**, 52-61.

(9) L. Zou, Q. Wu, Y. Zhou, X. Gong, X. Liu and F. Wang, *Chem. Commun.*, 2019, **55**, 6519-6522.